Microfluid Nanofluid (2011) 10:1175–1183
DOI 10.1007/s10404-010-0745-6

ORIGINAL PAPER

An experimental investigation of two-phase coating flow within microchannels: the effect of coating fluid rheology

Michael W. Boehm · Steven Sarker · Kurt Koelling

Received: 4 October 2010 / Accepted: 25 November 2010 / Published online: 18 December 2010

Abstract The study of multiphase flow within micro-scale geometries has garnered much attention in recent history. One system of interest is the flow of a low viscosity fluid thread, labeled as the coring fluid, through a much higher viscosity liquid, labeled the coating fluid. On the macro-scale, this process has shown great utility in the plastics industry, but it has yet to be completely characterized on the micro-scale. Detailed here is a set of experiments performed within square microchannels, of nominal area 250 μm by 250 μm, where the coring fluid was Newtonian and the coating fluid was either Newtonian or viscoelastic. Visual data were collected and subsequently analyzed to determine the thickness of coating fluid remaining on the walls of the microchannel after the coring fluid front passed. The results for flow through a Newtonian coating fluid show similarity to results for flow in macro-scale capillaries; the thickness of the coating fluid, after initial penetration by the coring fluid thread, follows the same dependence upon the velocity of the thread front as seen for the macro-scale. The case of a viscoelastic coating fluid in a microchannel, however, shows interesting differences to the macro-scale results. Most notably, the surface of the coring fluid thread was highly unstable and the entire thread migrated toward one wall.

M. W. Boehm · S. Sarker · K. Koelling (✉)
William G. Lowrie Department of Chemical and Biomolecular Engineering, The Ohio State University, Columbus, OH 43210, USA
e-mail: koelling@chbmeng.ohio-state.edu

Keywords Viscoelastic · Two-phase · Coating flow · Microfluidics

1 Introduction

The flow of a low viscosity thread through a much higher viscosity liquid within micro-scale geometries is an interesting topic in terms of what it can tell us about the fundamental yet complex relationships between geometry, interfacial tension, and shear forces. Presented here are experiments designed to extend the current understanding of two-phase coating flow within micro-scale architectures by studying two systems: (1) a Newtonian coating liquid and (2) a viscoelastic coating liquid, both of which are cored using a Newtonian liquid. The size, shape, and stability of the coring fluid thread will be examined and correlations made to the coring fluid flow rate.

1.1 Macro-scale coating flow

Fairbrother and Stubbs (1935), motivated by prior research of the electrically driven motion of a liquid through a membrane, determined the error between apparent and actual velocity when a small film of liquid lubricates a gas bubble flowing through a constriction. Fairbrother and Stubbs found that the error in velocity went with the square root of the Capillary number, Ca (Eq. 1). The findings, however, are only valid over a very small range of Ca. Taylor (1961) later took up the problem of capillary coating and his findings suggested that the fractional coverage (Eq. 2) approached a limiting value of $m = 0.56$. Cox (1962) found that the fractional coverage actually approached a limit of $m = 0.6$.

$$\mathrm{Ca} \equiv \frac{\mu U_{\mathrm{thread}}}{\sigma}, \tag{1}$$

$$m \equiv \frac{\mathrm{Area}_{\mathrm{geometry}} - \mathrm{Area}_{\mathrm{thread}}}{\mathrm{Area}_{\mathrm{geometry}}}. \tag{2}$$

Further work has confirmed previous conclusions (Bretherton 1961; Cox 1964; Schwartz et al. 1986; Gauglitz et al. 1987; Poslinski and Stokes 1993) and built upon the fundamental understanding by extending the coating experiment to include non-circular channels (Cerro et al. 1990; Cerro and Kolb 1991) and non-Newtonian coating fluids (Huzyak and Koelling 1997; Gauri and Koelling 1999a, b). The process has also been well studied from theoretical and numerical perspectives (Cox 1962; Goldsmith and Mason 1963; Saffman and McLean 1981; Khomami et al. 2004; Tsamopoulos and Dimakopoulos 2004; Feng 2009).

1.2 Multiphase microfluidics

Whitesides (2006) and Gunther and Jensen (2006) provide excellent reviews of microfluidics research currently underway. The simplest multiphase system involves Newtonian fluids (Guido et al. 2000; Chung and Kawaji 2004; Hwang et al. 2005; Garstecki et al. a, b; Vananroye et al. 2006; Fries et al. 2008; Weinmueller et al. 2009). Scientists have investigated more complex systems: including drop deformation (Chinyoka et al. 2005; Hsu and Leal 2009) and co-flowing systems (Khomami and Su 2000; Khomami et al. 2000; Husny and Cooper-White 2006; Steinhaus et al. 2007; Christopher and Anna 2009) involving a Newtonian phase and a viscoelastic phase.

2 Materials and experimental methods

There were two experimental sets performed and analyzed. The first was the simple case of a Newtonian liquid coring a Newtonian liquid. The second experimental set was a Newtonian liquid coring a viscoelastic liquid. The details of each experimental set are listed below, but a quick discussion of rheology is warranted before discussing the materials and methods.

2.1 Rheology

Rheology is the study of the flow and deformation of matter, but it is really about the drive to understand molecular-level interactions and the associated bulk-level behavior of matter when subjected to an outside force. On the macro-scale, the physical property of interest when investigating flow and deformation of liquids is the viscosity. Viscosity is the resistance to flow and arises directly from the interactions between neighboring molecules. The starting point, then, is with viscosity in its simplest form: the Newtonian fluid. A Newtonian fluid has a constant viscosity, except for changes in temperature or pressure. The equation for a Newtonian fluid in one dimension is shown below:

$$\tau \equiv \eta\dot{\gamma}. \tag{3}$$

The flux of momentum, τ, is related to the velocity gradient, $\dot{\gamma}$, by way of the viscosity, η. In addition to Newtonian fluids, there are many types of fluids that are not as simple and are, therefore, termed non-Newtonian. The research detailed below used two model fluids: a Newtonian fluid (Eq. 3) and a viscoelastic fluid. A viscoelastic fluid will act like a viscous liquid and an elastic solid. Viscoelastic fluids are composed of a low viscosity Newtonian liquid to which has been added an arbitrary weight fraction of high molecular weight (MW) polymer; the polymer chains can vary in molecular weight from hundreds to millions. The constitutive model for a viscoelastic fluid is considerably more complex than Eq. 3 because more empirical parameters are needed in order to accurately model the rheological response. The particular constitutive model used here is called the Giesekus model, though there are many other models. The Giesekus model in its general three-dimensional form is shown, in parts, in Eqs. 4a–c:

$$\vec{\vec{\tau}} \equiv \vec{\vec{\tau}}_{\mathrm{s}} + \vec{\vec{\tau}}_{\mathrm{p},i}, \tag{4a}$$

$$\vec{\vec{\tau}}_{\mathrm{s}} \equiv -\eta_{\mathrm{s}} 2\vec{\vec{D}}, \tag{4b}$$

$$\vec{\vec{\tau}}_{\mathrm{p},i} + \lambda_i \vec{\vec{\tau}}_{\mathrm{p1},i} - \alpha_i \frac{\lambda_i}{\eta_{\mathrm{p},i}} \left(\vec{\vec{\tau}}_{\mathrm{p},i} \cdot \vec{\vec{\tau}}_{\mathrm{p},i} \right) \equiv -\eta_{\mathrm{p},i} 2\vec{\vec{D}}. \tag{4c}$$

The Giesekus model includes contributions from the solvent and polymer, τ_s and τ_p respectively, by including empirical fitting constants for the polymer relaxation time, λ, a drag coefficient, α, and the polymer contribution to the shear viscosity, η_p. The practical form of the Giesekus model, however, involves multiple modes. By modes, it is meant sets of empirical constants. For instance, a 4-mode Giesekus model offers 12 total empirical constants, the three constants listed above for each of the four total modes. Practically speaking, a multi-mode Giesekus model is more useful because steady and dynamic shear as well as extensional flow can be modeled more accurately.

2.2 Materials

The materials used in all experiments as well as their respective function and physical properties are listed in Table 1. The property values listed are taken at ~25°C and all experiments were performed at ~25°C with the

Table 1 Physical properties and functions for materials

Experiment/properties	Fluid name, type, function	Density (g/ml)	Viscosity (Pa s)	Viscosity ratio	Interfacial Tension (N/m)
Newtonian coating	Silicone oil, Newtonian, coring fluid	0.940	0.009	8000	~0.0033
	Polybutene, Newtonian, coating fluid	0.89	72		
Viscoelastic coating	Water, Newtonian, coring fluid	1	0.001	9000	0.031
	PIB in PB, viscoelastic, coating fluid	0.88	9		

assumption that density, viscosity, and interfacial tension changed little with changes in room temperature. The microchannels were all μ-CNC machined into poly (methyl methacrylate), PMMA, with a nominal cross-sectional area of 250 μm by 250 μm. The machined microchannels were imaged under a microscope with a 20× lens in order to assess surface roughness and channel width. The channels with rough sidewalls were not used. The only additional measurement of microchannel dimension was made during data analysis and only the microchannel width was measured as it was easily visualized. Future work will aim to measure the coring thread and microchannel cross-sectional area. For the purposes of this article, only conclusions pertaining to the coring thread width will be made.

2.2.1 *Newtonian coating*

Silicone oil (F10, Brookfield Engineering) was used as the coring fluid and polybutene (H-300, Indopol) was used as the coating fluid, both of which were used as received. The silicone oil was a rheometer grade test fluid. The oil was tested under simple shear at 25°C with a parallel plate setup. The viscosity matched that listed by the manufacturer and showed Newtonian behavior. The density value was obtained from the manufacturer's web site. The coating fluid was a low molecular weight polybutene and also tested under simple shear at 25°C with a parallel plate setup. The density was obtained from the manufacturer's product information.

The interfacial tension for the silicone oil/polybutene system was averaged using two values found in the literature (Guido et al. 2000; Cristini et al. 2002), with one caveat. The work of Guido et al. and Cristini et al. used silicone oils and polybutenes of higher molecular weight than were used for this article. There are reports of interfacial tension for systems involving various chain-length liquids and the interfacial tension does change. Regardless, the assumption was made that the value used here is a faithful Order of Magnitude representation.

2.2.2 *Viscoelastic coating*

The Newtonian coring fluid was water with blue food coloring added (*for better visualization*). A simple parallel plate setup and steady shear was used to verify that the blue dye did not alter the viscosity of the water and the density was taken simply as that of water, both values taken at 25°C. The coating fluid was a viscoelastic fluid, commonly called a Boger fluid. The Boger fluid was made by mixing polyisobutylene into polybutene at 0.25% w/w. The exact mixing procedure and formulation can be found elsewhere (Gauri 1999).

The interesting aspect of the Boger fluid is that elastic properties are present without the accompanying shear thinning in the shear viscosity. This is beneficial, and even desired, for coating experiments because the effect on the fractional coverage of a shear thinning coating fluid counters the effect of a viscoelastic fluid. Considering Fig. 3, the fractional coverage for a shear thinning fluid negatively diverges from the Newtonian fluid values. At high *Ca*, the fractional coverage first drops for a shear thinning fluid then asymptotes at a value lower than the Newtonian asymptote. For a viscoelastic fluid, however, the fractional coverage continues to increase with increases in *Ca*. If a viscoelastic fluid showing elasticity and shear thinning properties were used, the results would be a function of both the shear viscosity and the elasticity, which is not preferred in a study of this nature.

The steady shear data as well as Giesekus model fits are shown in Fig. 1. The Giesekus model allows various "modes," which means nothing more than how many total fitting parameters are used.

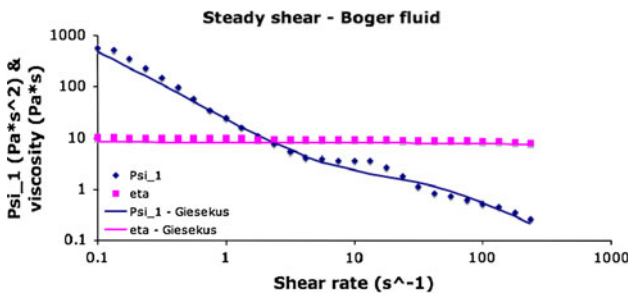

Fig. 1 Steady shear data for a viscoelastic fluid with Giesekus model fit

$$X_i \equiv \sum \left(\frac{\left(1 + 16\alpha_i(1-\alpha_i)(\lambda_i\dot{\gamma})^2\right)^{0.5} - 1}{8\alpha_i(1-\alpha_i)(\lambda_i\dot{\gamma})^2} \right)^{0.5}, \quad (5a)$$

$$f_i \equiv \sum \frac{1 - X_i}{1 + (1-2\alpha_i)X_i}, \quad (5b)$$

$$\Psi_1 \equiv \sum \frac{\eta_i f_i (1 - \alpha_i f_i)}{\lambda_i \dot{\gamma}^2 \alpha_i (1 - f_i)}, \quad (5c)$$

$$\eta_p \equiv \sum \frac{\eta_i (1 - f_i)^2}{1 + (1-2\alpha_i) f_i}. \quad (5d)$$

For instance, the fit in Fig. 1 was made via a 4-mode model (Eqs. 5a–d). This means there are four instances of the parameters η, the polymer contribution to the viscosity, λ, the relaxation time, and α, an interaction parameter that accounts for the drag on the polymer chains by the continuous phase. The Giesekus model must be fit to the data, but because there are only three parameters (multiplied by the number of modes being used) that have to be fit to three entirely different flow regimes the model will only fit all regimes reasonably well or the model can fit one regime very well and the others only reasonably well. First, by flow regime it is meant steady shear, dynamic shear, or extensional flow. Second, to which regime the model is fit best is dependent upon the experimental system being studied. For instance, the flow regimes present in the experiments detailed in the following sections were extensional and steady shear. However, the results were analyzed based on the Deborah number, *De* (Eqs. 9a, b), and it is calculated using ψ_1, which is a value obtained in steady shear. Therefore, the Giesekus model was fit to the steady shear data. Additional information concerning the Giesekus model and fits to it can be found elsewhere (Bird and Wiest 1985; Giesekus 1982; Shackleford 1996; Quinzani et al. 1990).

The interfacial tension data for this system was taken from previous work (Gauri 1999) with the assumption that the blue dye did not alter the value.

2.3 Experimental method

All experiments were performed following the same general procedure and using the same microchip design (nominal cross-sectional area of 250 μm by 250 μm), both of which are illustrated in Fig. 2. Due to the variability in machining, the microchannel width varied anywhere from 250 to 300 μm, with the average channel width being about 265 μm.

The coating fluid was manually injected, using a standard 10 ml plastic syringe, from the far left hole and stopped immediately before reaching the intersection. The syringe was removed and then another 10 ml plastic syringe filled with the coring fluid was attached to the hole at far right. The coring fluid was manually injected until it exited the exhaust hole located at the end of the side channel. The plastic syringe was removed, a glass syringe of either 10 or 100 μl volume containing the coring fluid was attached to the hole at the far right and then epoxy was applied to the exhaust hole. At this point, the microchip was moved to the microscope and the syringe was connected to the pump. With the syringe in place, the epoxy was given time to cure. The chip was placed such that the middle of the microchannel was in the microscope's field of view. This was done to ensure no effect from the channel entrance or exit and so all video would be taken at the same location.

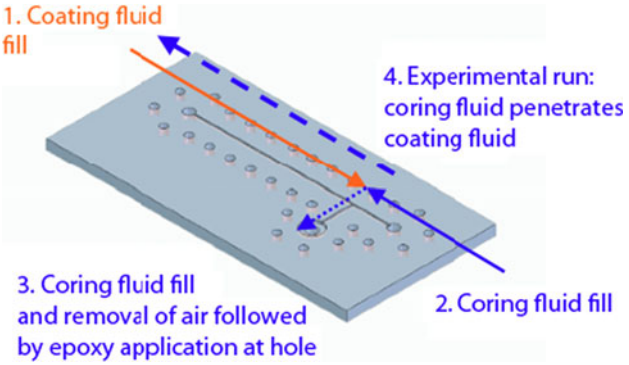

Fig. 2 Illustration of the coating process

For experiments involving the viscoelastic coating fluid, the coring fluid flow was not started until 15 min after the coating fluid was injected. This was done to ensure that the polymer chains had ample time to relax, which could be seen as a moving contact line and normally occurred about 5 min after filling the coating fluid. This is a small step but important because residual stress on the polymer chains results in an additional, unintended response from the coring fluid thread.

Once the epoxy had cured, the coring fluid flow was started and the video capture software was turned on. Video was taken at the same settings for all experiments. In general, the video was captured at least until the thread front completely passed the field of view and at most for 4 min total. The software was then switched off, the pump stopped, and the chip discarded.

3 Results and discussion

The driving focus of this article was to examine the dynamics of coating flow within microchannels and to compare those results to what is known for the macro-scale. Historical results collected within our group for coating flow in macro-scale capillaries are shown in Fig. 3

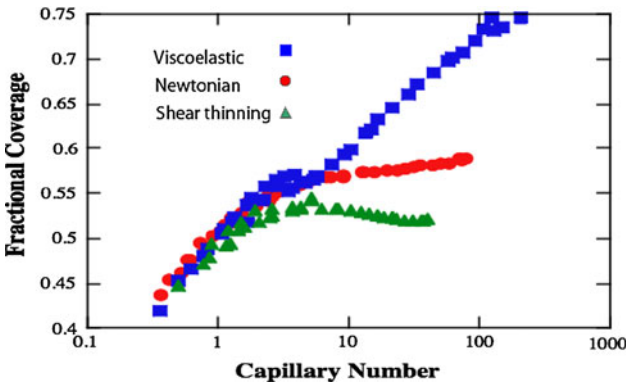

Fig. 3 Fractional coverage graphed versus Capillary number for flow in a macro-scale capillary. The *blue squares* represent flow through a viscoelastic coating fluid, *green triangles* for flow through a shear thinning coating fluid, and *red dots* for flow through a Newtonian coating fluid (reprinted from Gauri 1999 with permission). (Color figure online)

(Gauri 1999). The triangles represent data collected for a shear thinning coating fluid and squares represent data for a viscoelastic coating fluid. The circles are the Newtonian coating fluid results showing an asymptotic limit in fractional coverage. The shear thinning fluid shows negative divergence from the Newtonian case because the higher *Ca* is marked by higher shear rates, which results in a decreasing coating fluid viscosity. The decreasing viscosity gives a decreasing shear stress and because the stress counters the interfacial tension larger threads result. Conversely, the viscoelastic fluid shows marked increases in stress (actually normal forces) with increasing *Ca*. The increased stress results in smaller thread shapes and hence larger coatings.

3.1 Data collection and data analysis

The results presented below were obtained from video. Conventional PC-based video capture software was used to record *avi* files for later play back. The video files were used in two ways: (1) to calculate the bubble velocity within the video frame and (2) to export individual images for subsequent use in Photoshop. The video file was used to calculate the thread velocity. The individual images were used to calculate the thread width, the channel width, and the total distance traveled by the thread front. A conversion between pixels and micrometer was calculated based on the microscope calibration. Figure 4 is a representative image created in Photoshop showing the thread front at two locations in the video frame.

The next step was to crop the images to rectangles of 184 (H) by 216 (W) pixels, take the inverse, and save in *bmp* format for use in a custom Matlab program. The Matlab program was used to fit a function to the shape of the thread front. An edge detection algorithm (Canny 1986)

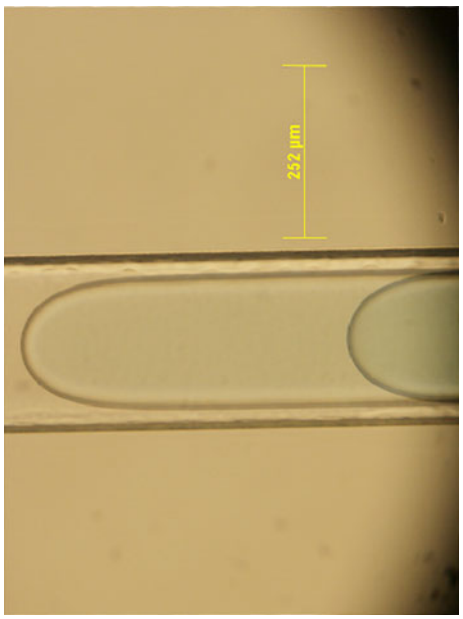

Fig. 4 Composite image of the moving thread front

was used in conjunction with manual deletion to find the edge of the thread and remove all remaining edges. The values representing the surface were then fit using a 6-mode Fourier transform. In almost all cases, the fit was smooth and accurately represented the thread front shape.

3.2 Newtonian coating

The results for a Newtonian coating fluid are shown in Fig. 5, graphed as normalized thread diameter ($D_N = D_{thread}/D_{Channel}$) versus *Ca*. The line represents the macro-scale Newtonian coating fluid results of Gauri (1999). The boxes are the results obtained here. The general trend for decreased normalized thread diameter with increased *Ca* is clear.

The data in Fig. 5 are qualitatively and quantitatively similar to that obtained on the macro-scale and could be used to conclude that the dynamics have not changed. Making this conclusion would be unwise, though. The interfacial tension actually plays a more important role on the micro-scale but only in conjunction with the channel design (*channel design encompasses geometry*). The same fluids and the same thread front velocities will show different flow patterns if a different channel design is used. Interestingly, *Ca* is independent of geometry thus offering no explicit insight into how the thread front shape develops, changes, and is affected by the physical structure of the channel.

$$Re \equiv \frac{\rho d V}{\eta}, \tag{6}$$

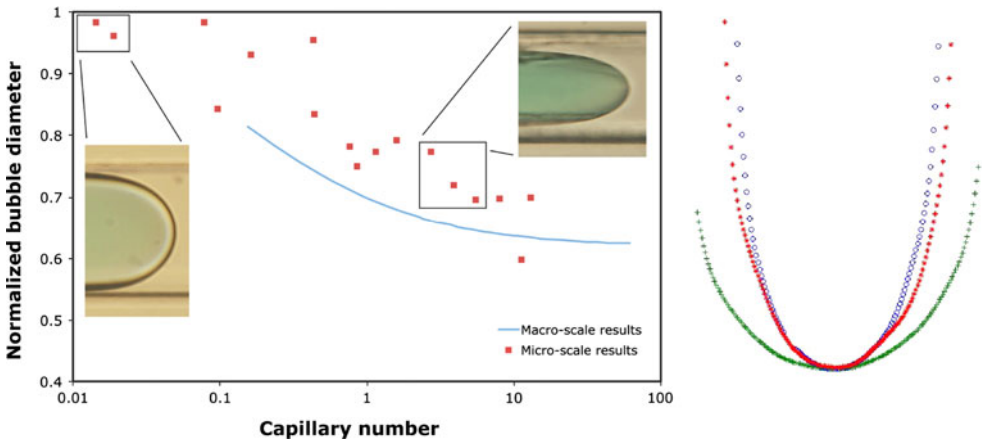

Fig. 5 *Left pane* Normalized thread diameter graphed versus *Ca* for coating flow through a Newtonian coating fluid. The *red squares* are the data collected for flow in a microchannel, the *blue line* represents the data for flow in a macro-scale capillary, and the *inset photos* are of the coring threads at low (*left photo*) and high (*right photo*) *Ca* in a microchannel. *Right pane* Thread front shape graphed for $Ca = 0.43$, 1.6, 13 (*green* "+", *red* "*", *purple* "o"). The microchannel width for the three fronts shown were 254, 245, and 261 μm, respectively. Notice the residual periodicity, in the middle line—*red stars*—from the Fourier transform fitting. (Color figure online)

$$We \equiv \frac{V^2 R\rho}{\sigma}, \tag{7}$$

$$St \equiv \frac{\Delta\rho g R^2}{U_b \eta}. \tag{8}$$

In the above equations, the factors include density, ρ, characteristic lengths, d and R, characteristic velocities, V and U_b, viscosity, η, and interfacial tension, σ. To further support the conclusion that viscous and interfacial tension forces dominate, the Reynolds number, *Re*, and the Weber number, *We*, range between 10^{-10} and 2×10^{-4}. The Reynolds number gives the relative importance of inertial forces to viscous forces and the Weber number gives the relative importance of inertial forces to interfacial tension forces. The conclusion can be made that inertial forces are unimportant when compared to viscous and interfacial tension forces. As for gravitational forces, the Stokes number, *St*, ranged between $\sim 10^{-4}$ and $\sim 10^{-2}$ supporting the claim that gravitational forces are also not important compared to viscous and interfacial tension forces.

The viscosity ratio is another important topic to discuss. The ratio of coating fluid to coring fluid viscosity for both systems was $\sim 10^4$, which means in theory the coring fluid can be considered inviscid—without viscosity. Such a large ratio is useful because the coring fluid does not impart flow once the thread front has passed. In other words, the coating fluid within the coating layer has zero velocity. In essence, this means that the coating thickness is determined by the dynamics at the thread front and not what happens after it passes. In a microchannel, this assumption does not necessarily hold and determining how much motion exists in the coating layer is one topic for future study.

A good technique for determining the dynamics at the thread front without additional flow visualization equipment is to compare the front shape as a function of *Ca*. The first step was to compare the front shape for both photos taken from an individual experiment. This was done to ensure that the front shape, and hence the front velocity, was constant within the video frame. The next step was to compare front shapes as a function of *Ca*. The right pane of Fig. 5 displays a range of front shapes. The front shape comparison illustrates the graphical information shown on the left pane in Fig. 5: higher *Ca* results in smaller thread front diameters. Also, additional information of how the front tip is shaped by the flow can be gleaned from the comparison. The increasing *Ca* is just another way of stating that the viscous forces are becoming as or more important than interfacial tension forces. The higher viscous forces create stress on the front surface and sharpen the tip, making the front more streamlined. Conversely, the lowest *Ca* is marked by a dominant interfacial tension force thus the front surface is far more rounded.

The results for a Newtonian coating fluid match the macro-scale results. It would at first seem as if viscous and interfacial tension forces become more important as the size of the channel is reduced. The quantitative and qualitative similarity between the micro-scale and macro-scale results can be used to make the suggestion that the dynamics are the same. In general, this is a good conclusion, but the synergy between channel design and interfacial tension can drive the system toward instability.

3.3 Viscoelastic coating

The results for a viscoelastic coating fluid within a microchannel are shown in Fig. 6. Similar to the case of flow within a macrocapillary (Fig. 3), the fractional coverage, or

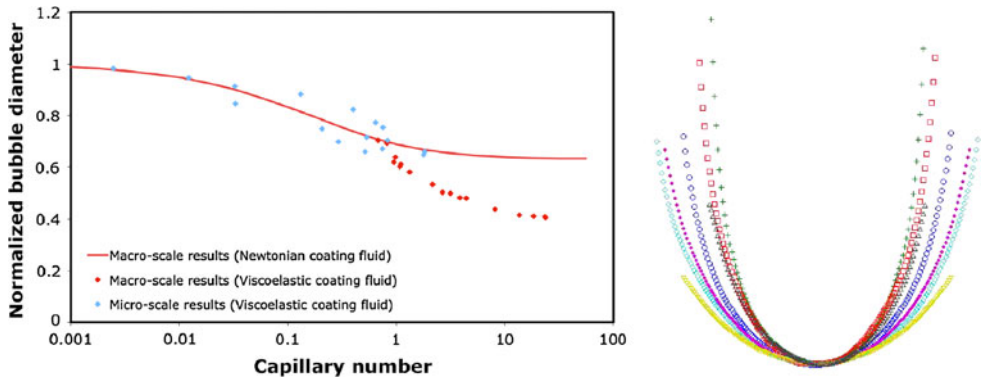

Fig. 6 *Left pane* Normalized thread diameter graphed versus *Ca* for coating flow through a viscoelastic coating fluid (*Diamonds* for flow in a microchannel, *squares* for flow in a macrocapillary). The *line* represents the historical data for flow through a Newtonian coating fluid in a macro-scale capillary. *Right pane* Thread front shape graphed for *Ca*, within the range $Ca = 0.02$–2, for flow through a viscoelastic coating fluid, where the widest front shape corresponds to the smallest *Ca*. The average microchannel width for the thread fronts shown was 275 ± 15.5 μm. (Color figure online)

inversely the normalized thread diameter, falls onto the same curve as a Newtonian coating fluid, for low *Ca*. For comparison, the left pane of Fig. 6 includes data points for a viscoelastic coating fluid in a 1 mm diameter macrocapillary (Gauri 1999). The data for microchannel flow were expected to follow the trend shown by the squares, i.e. divergence from the Newtonian line. Unfortunately, the experiments presented here did not reach the higher flow rates shown in Fig. 3, which motivates an important question, "Why not?"

Interestingly, the highest volumetric flow rate for the viscoelastic coating fluid experiments was 1 ml/min yet the measured thread front velocity was only 0.006 m/s, which can be compared to a volumetric flow rate of 150 μl/min and a measured thread front velocity of 0.012 m/s for a Newtonian coating fluid. For reference, there was no leakage from the microchip, pump, or syringe during the 1 ml/min experiment. The common understanding stipulates an increased front velocity results when the volumetric flow rate is increased, for equal areas. Drawing from the entire set of thread velocity data for flow through a viscoelastic fluid (*data not shown*), there would appear to be a limit to the velocity. However, further data must be collected before making a final conclusion.

Thus far, only data for the thread front and a short distance behind it have been presented. Additional video data were captured of the thread far upstream of the front (*data not shown*). The thread, regardless of *Ca*, travels smoothly very near the front. However, at a short time there may or may not be disturbances in the thread. There appears to be a low $Ca \sim 0.5$ limit below which the thread shape is smooth and disturbance free. In the range $0.5 < Ca < 0.7$, the thread suffers from slight disturbances in the form of traveling waves. Above $Ca \sim 0.7$, the thread suffers from extreme disturbances in the form of waves and near snap-off as well as bulk migration. Bulk migration involves the entire thread shifting position toward one of the walls. On its own, the migration could be attributed to gravitational effects (though it is not proposed to be the cause). The migration coupled with the traveling disturbances suggests more complex dynamics are at work. It is hypothesized that slight asymmetries in the thread's position resulted in one side of the thread experiencing a larger force. It is known that particles or bubbles traveling in a tube filled with a viscoelastic fluid will migrate toward the walls under the right conditions (Binous and Phillips 1999). The same dynamics could be at play in this system. This hypothesis is strengthened by the fact that there are traveling waves along the thread. The elastic forces at the higher flow rates are large enough to nearly collapse the thread. The dynamic nature of the traveling wave could produce an unstable and unsteady system.

$$De \equiv \frac{\lambda}{\mathrm{t}} \equiv \lambda \dot{\gamma}_{\mathrm{w}} \equiv \frac{\Psi_1(\dot{\gamma}_{\mathrm{w}})}{2\eta_{\mathrm{p}}}\dot{\gamma}_{\mathrm{w}}, \tag{9a}$$

$$\dot{\gamma}_{\mathrm{w}} \equiv \frac{2U_{\mathrm{thread}}}{a}. \tag{9b}$$

The Deborah number, *De*, is a ratio of the polymer relaxation time, λ, to a characteristic time, *t*. The characteristic time is calculated as the wall shear rate, $\dot{\gamma}_{\mathrm{w}}$, which is simply twice the thread front velocity divided by the channel half-width, *a*. The polymer relaxation time can also be represented by the first normal stress coefficient, Ψ_1, divided by twice the polymer contribution to the shear viscosity, η_{p}. The first normal stress coefficient is shear rate dependent and can be calculated using the Giesekus model fit to steady shear data.

Using *De*, it was found that the transition to unsteady flow occurred at progressively higher *De*. The fact that the

thread transitions with higher *De* supports the conclusion that elastic effects cause the instability because the higher the *De* the less time available for the polymer chains to relax and thus the larger the normal forces generated by the stretched polymer chains.

To end, let it be said that high flow rates in Newtonian fluids show no such thread instabilities. The coring process was investigated for a viscoelastic coating fluid and compared to macro-scale results and micro-scale results for Newtonian coating fluids. In general, the coring process shows the same dynamics as on the macro-scale. However, the data can be used to suggest that the elastic properties become more important as the channel size is decreased.

4 Conclusions

Presented here were data for two-phase coating flow within a square 250 μm channel: where the coating fluid was either (1) Newtonian, or (2) viscoelastic. Conventional video acquisition was used to record thread front velocities and thread shapes during the coating process. The trends in thread shape show similarity to the historical macrocapillary data. However, the case of a viscoelastic coating fluid presented behavior not witnessed on the macro-scale, namely, instabilities in the coring thread shape and a maximum thread front velocity. These data add to the current understanding of two-phase flow, but they do not complete the picture. For instance, the full cross-sectional thread shape should be imaged and further experiments designed to probe the instability witnessed when using a viscoelastic coating liquid.

Acknowledgments This work was supported by NSF Grant EEC-0425626, Center for Affordable Nanoengineering of Polymeric Biomedical Devices, The Ohio State University. All rights reserved.

References

Binous H, Phillips RJ (1999) The effect of sphere-wall interactions on particle motion in a viscoelastic suspension of FENE dumbbells. J Non Newton Fluid Mech 85:63–92

Bird RB, Wiest JM (1985) Anisotropic effects in dumbbell kinetic theory. J Rheol 29:519–532

Bretherton FP (1961) The motion of long bubbles in tubes. J Fluid Mech 10:166–188

Canny J (1986) A computational approach to edge detection. IEEE Trans Pattern Anal Mach Intell PAMI 8:679–697

Cerro RL, Kolb WB (1991) Coating the inside of a capillary of square cross section. Chem Eng Sci 46:2181–2195

Cerro RL, Sublette KL, Kolb WB, Camp CE (1990) The measurement of square channel velocity profiles using a microcomputer-based image analysis system. Exp Fluids 10:87–92

Chinyoka T, Renardy YY, Renardy M, Khismatullin DB (2005) Two-dimensional study of drop deformation under simple shear for Oldroyd-B liquids. J Non Newton Fluid Mech 130:45–56

Christopher GF, Anna SL (2009) Passive breakup of viscoelastic droplets and filament self-thinning at a microfluidic T-junction. J Rheol 53:663–683

Chung PMY, Kawaji M (2004) The effect of channel diameter on adiabatic two-phase flow characteristics in microchannels. Int J Multiph Flow 30:735–761

Cox BG (1962) On driving a viscous fluid out of a tube. J Fluid Mech 14:81–96

Cox BG (1964) An experimental investigation of the streamlines in viscous fluid expelled from a tube. J Fluid Mech 20:193–200

Cristini V, Hooper RW, Macosko CW, Simeone M, Guido S (2002) A numerical and experimental investigation of lamellar blend morphologies. Ind Eng Chem Res 41:6305–6311

Fairbrother F, Stubbs AE (1935) Studies in electro-endosmosis. Part VI. The 'Bubble-tube' method of measurement. J Chem Soc 1:527–529

Feng JQ (2009) A long gas bubble moving in a tube with flowing liquid. Int J Multiph Flow 35:738–746

Fries DM, Trachsel F, von Rohr PR (2008) Segmented gas-liquid flow characterization in rectangular microchannels. Int J Multiph Flow 34:1108–1118

Garstecki P, Fuerstman MJ, Stone HA, Whitesides GM (2006a) Formation of droplets and bubbles in a microfluidic T-junction—scaling and mechanism of break-up. Lab Chip 6:437–446

Garstecki P, Fuerstman MJ, Fischbach MA, Sia SK, Whitesides GM (2006b) Mixing with bubbles: a practical technology for use with portable microfluidic devices. Lab Chip 6:207–212

Gauglitz PA, Ransohoff TC, Radke CJ (1987) Snap-off of gas bubbles in smoothly constricted noncircular capillaries. AIChE J 33:753–765

Gauri V (1999) The penetration of a long bubble through viscous and viscoelastic fluids in capillary tubes. Dissertation, The Ohio State University

Gauri V, Koelling K (1999a) Gas-assisted displacement of viscoelastic fluids: flow dynamics at the bubble front. J Non Newton Fluid Mech 83:183–203

Gauri V, Koelling K (1999b) The motion of long bubbles through viscoelastic fluids in capillary tubes. Rheol Acta 38:458–470

Giesekus H (1982) A simple constitutive equation for polymer fluids based on the concept of deformation-dependent tensorial mobility. J Non Newton Fluid Mech 11:69–109

Goldsmith HL, Mason SG (1963) The flow of suspensions through tubes II. Single large bubbles. J Colloid Sci 18:237–261

Guido S, Minale M, Maffettone PL (2000) Drop shape dynamics under shear-flow reversal. J Rheol 44:1385–1399

Gunther A, Jensen KF (2006) Multiphase microfluidics: from flow characteristics to chemical and materials synthesis. Lab Chip 6:1487–1503

Hsu AS, Leal LG (2009) Deformation of a viscoelastic drop in planar extensional flows of a Newtonian fluid. J Non Newton Fluid Mech 160:176–180

Husny J, Cooper-White JJ (2006) The effect of elasticity on drop creation in T-shaped microchannels. J Non Newton Fluid Mech 137:121–136

Huzyak PC, Koelling K (1997) The penetration of a long bubble through a viscoelastic fluid in a tube. J Non Newton Fluid Mech 71:73–88

Hwang JJ, Tseng FG, Pan C (2005) Ethanol-CO_2 two-phase flow in diverging and converging microchannels. Int J Multiph Flow 31:548–570

Khomami B, Su KC (2000) An experimental/theoretical investigation of interfacial instabilities in superposed pressure-driven channel flow of Newtonian and well characterized viscoelastic fluids Part I: linear stability and encapsulation effects. J Non Newton Fluid Mech 91:59–84

Khomami B, Renardy Y, Su KC, Clarke MA (2000) An experimental/theoretical investigation of interfacial instabilities in superposed pressure-driven channel flow of Newtonian and well characterized viscoelastic fluids Part II: nonlinear stability. J Non Newton Fluid Mech 91:85–104

Khomami B, Shaqfeh ESG, Bhatara G (2004) Influence of viscoelasticity on the interfacial dynamics of air displacing fluid flows—a computational study. J Non Newton Fluid Mech 122:313–332

Poslinski AJ, Stokes VK (1993) Gas-assisted displacement of a viscous liquid in a tube. Proc ANTEC 39:68–73

Quinzani LM, McKinley GH, Brown RA, Armstrong RC (1990) Modeling the rheology of polyisobutylene solutions. J Rheol 34:705–748

Saffman PG, McLean JW (1981) The effect of surface tension on the shape of fingers in a Hele Shaw cell. J Fluid Mech 102:455–469

Schwartz LW, Princen HM, Kiss AD (1986) On the motion of bubbles in capillary tubes. J Fluid Mech 172:259–275

Shackleford DS (1996) Transient shear and extensional rheology of dilute and semi-dilute polymer solutions. Dissertation, The Ohio State University

Steinhaus B, Shen AQ, Sureshkumar R (2007) Dynamics of viscoelastic fluid filaments in microfluidic devices. Phys Fluids 19:073103-1–073103-13

Taylor GI (1961) Deposition of a viscous fluid on the wall of a tube. J Fluid Mech 10:161–165

Tsamopoulos J, Dimakopoulos Y (2004) On the gas-penetration in straight tubes completely filled with a viscoelastic fluid. J Non Newton Fluid Mech 117:117–139

Vananroye A, Puyvelde PV, Moldenaers P (2006) Effect of confinement on droplet breakup in sheared emulsions. Langmuir 22:3972–3974

Weinmueller C, Hotz N, Mueller A, Poulikakos D (2009) On two-phase flow patterns and transition criteria in aqueous methanol and CO_2 mixtures in adiabatic, rectangular microchannels. Int J Multiph Flow 35:760–772

Whitesides GM (2006) The origins and the future of microfluidics. Nature 442:368–373